Available online at www.sciencedirect.com
ScienceDirect
Journal of Power Sources 167 (2007) 358–365
JOURNAL OF POWER SOURCES
www.elsevier.com/locate/jpowsour

Investigations of direct methanol fuel cell (DMFC) fading mechanisms

Loka Subramanyam Sarma [a], Ching-Hsiang Chen [a], Guo-Rung Wang [a], Kan-Lin Hsueh [c], Chiou-Ping Huang [c], Hwo-Shuenn Sheu [b], Ding-Goa Liu [b], Jyh-Fu Lee [b], Bing-Joe Hwang [a,b,*]

[a] *Nanoelectrochemistry Laboratory, Department of Chemical Engineering, National Taiwan University of Science and Technology, Taipei 106, Taiwan, ROC*
[b] *National Synchrotron Radiation Research Center, Hsinchu 30076, Taiwan, ROC*
[c] *Industrial Technology Research Institute, Hsinchu 310, Taiwan, ROC*

Received 1 January 2007; received in revised form 6 February 2007; accepted 8 February 2007
Available online 21 February 2007

Abstract

In this report, we present the microscopic investigations on various fading mechanisms of a direct methanol fuel cell (DMFC). High energy X-ray diffraction (XRD), X-ray absorption spectroscopy (XAS), energy dispersive X-ray spectroscopy (EDX), and Raman spectroscopic analysis were applied to a membrane-electrode-assembly (MEA) before and after fuel cell operation to figure out the various factors causing its fading. High energy XRD analysis of the fresh and faded MEA revealed that the agglomeration of the catalyst particles in the cathode layer of the faded MEA was more significant than in the anode layer of the faded MEA. The XAS analysis demonstrated that the alloying extent of Pt (J_{Pt}) and Ru (J_{Ru}) in the anode catalyst was increased and decreased, respectively, from the fresh to the faded MEA, indicating that the Ru environment in the anode catalyst was significantly changed after the fuel cell operation. Based on the X-ray absorption edge jump measurements at the Ru K-edge on the anode catalyst of the fresh and the faded MEA it was found that Ru was dissolved from the Pt-Ru catalyst after the fuel cell operation. Both the Ru K-edge XAS and EDX analysis on the cathode catalyst layer of the faded MEA confirms the presence of Ru environment in the cathode catalyst due to the Ru crossover from the anode to the cathode side. The changes in the membrane and the gas diffusion layer (GDL) after the fuel cell operation were observed from the Raman spectroscopy analysis.

Keywords: Direct methanol fuel cell; Fading mechanism; Ru dissolution; X-ray absorption spectroscopy; Nafion degradation; Gas diffusion layer

1. Introduction

Low-temperature solid polymer electrolyte fuel cells such as direct methanol fuel cells (DMFCs) are gaining more and more attention from both scientific and technological perspectives due to their promising application for fuel cell vehicles, stationary applications, and portable power sources [1,2]. DMFC simplify the fuel cell system by operating without any external bulky fuel-reforming system and therefore would result in its rapid commercialization. With significant research efforts made on the development of electrocatalyst materials, proton exchange membranes, and modeling and design of cell components and complete stacks for DMFC from the past two decades [3–5], the performance achieved for the state-of-the art membrane and electrode assemblies (MEAs) in DMFCs can compete favorably with hydrogen-fueled and on-board reforming fuel cell systems [6,7]. However, the long-term stability of MEAs is of significant concern due to the degradation of cell components in either oxidizing or reducing environments accompanied with electrochemical potentials induced by the cell reactions. Targeted life time and failure testing can be conducted during the development stage, to provide the basis to understand potential failure mechanisms and develop the necessary technology to mitigate such mechanisms. Despite the key role that long-term stability is to have for the commercial success of DMFCs, only few publications appeared concerning the degradation effects in the MEAs. Thomas et al. have studied several factors affecting the performance of DMFCs particularly focusing on the long-term stability of the anode and crossover of methanol [8]. They have reported a 2000 h life time test at 0.4 V and 100 °C and found

* Corresponding author. Fax: +886 2 27376644.
E-mail address: bjh@mail.ntust.edu.tw (B.-J. Hwang).

0378-7753/$ – see front matter © 2007 Elsevier B.V. All rights reserved.
doi:10.1016/j.jpowsour.2007.02.020

12% loss in cell performance and suggested that the decay in the overall performance might be due to a slow drop in the anode activity. However, the factors responsible for drop in the anodic activity were not discussed. In another report durability-test data for the DMFC at 90 and 60 °C at a load current-density of 100 mA cm^{-2} in an 8 h test was also presented [9]. The authors found that the DMFC operating at 90 °C maintain its initial output voltage whereas operation at 60 °C showed a marked decay in its output voltage. They attributed the performance loss at 60 °C to the flooding of the cathode. In their study Yi and co-workers have carried out a 75 h life test of a DMFC at 100 mA cm^{-2} [10]. They found that 30% of the original maximum power density was lost after a 75 h life test and attributed the performance degradation of the DMFC to the agglomeration of electrocatalysts together with the delamination of the MEA. Even though most of the literature studies are focused on long-term fuel cell operation and highlighted some reasons for failure mechanisms, however the reasons for the degradation of single cell performance during long-term operation are still ambiguous to date. Hence, we believe that the studies focusing on exploring the various factors causing the failure of DMFC and some key evidence for their existence and their mechanisms are of great importance. Such efforts could contribute reasonably to optimize the various processes occurring in the DMFC operation and can achieve higher performance for the targeted applications. Hence, herein we have presented microscopic investigations of a MEA via various analytical techniques such as XRD, XAS, EDX, and Raman spectroscopy before and after DMFC operation. These microscopic investigations will provide a deep insight into the fading mechanism of a MEA in DMFC operation.

2. Experimental

2.1. Single cell testing

The DMFC single cell tests were performed with a DuPont™ membrane electrode assembly with an active geometric area of 9 cm^2 incorporated into a single cell testing fixture supplied by Asia Pacific Fuel Cell Technologies Ltd. The MEA was made with a Nafion® 117 membrane. The anode catalyst was a Pt-Ru black (1:1 ratio) and the cathode catalyst was a Pt black. The polarization curves were obtained using a fuel cell test system from Beam Technology after the single cell was operated for 600 h. The cell was operated under a 0.8 A load. Methanol feed concentration supplied to the anode was 2.5 M with a flow rate of 0.366 cm^3 min^{-1} by a Micro Diaphragm liquid pump and the cathode is fed with dry air with a flow rate of 75 cm^3 min^{-1}. All measurements were done at 40 °C and both anode and cathode were operated at atmospheric pressures. After the fading tests, the MEA was carefully removed from the cell and dried. The dried MEA sample was then cut into small pieces, which were used for the subsequent XRD, XAS, EDX, and Raman studies.

2.2. High energy X-ray diffraction (XRD) measurements

The high energy XRD measurements were performed on the fresh and faded MEA at the beam line BL01C2 at the NSRRC, Hsinchu, Taiwan. The beam line was operated with energy of 25 keV. The XRD pattern was recorded using the wavelength (λ) of 0.5167 Å for limited angular regions at room temperature. The wavelength has been changed to 1.5418 Å as the energy of Cu Kα. A single crystal of Si (1 1 1) with about 10% asymmetric cutting was used to deliver a monochromatic beam with a size of 1 mm in diameter with a single spot at the sample, which is about 24 and 6 m away from the source and monochromator, respectively. Flat imaging plate was used as a 2D area detector, which can collect diffraction pattern of the 2θ scale up to 40°. The XRD pattern was read out by a MAC IPR 420 off line imaging plate scanner.

2.3. X-ray absorption spectroscopy (XAS) measurements

The X-ray absorption spectra were recorded on the fresh and the faded MEA at the Taiwan beam line of BL01C1 at the NSRRC, Hsinchu, Taiwan. The electron storage ring was operated at 1.5 GeV. A double Si (1 1 1) crystal monochromator was employed for energy selection with a resolution $\Delta E/E$ better than 1×10^{-4} at both the Pt L_{III}-edge (11564 eV) and the Ru K-edge (22117 eV). Three gas-filled ionization chambers were used in series to measure the intensities of the incident beam (I_0), the beam transmitted by the sample (I_t), the beam subsequently transmitted by the reference foil (I_r). The third ion chamber was used in conjunction with the reference sample, which was a Pt foil for the Pt L_{III}-edge measurements and Ru powder for the Ru K-edge measurements. The control of parameters for EXAFS measurements, data collection modes and calculation of errors were all done as per the guidelines set by International XAFS Society Standards and Criteria Committee [11,12].

2.4. XAS data analysis

Standard procedures were followed to analyze the XAS data. First, the raw absorption spectrum in the preedge region was fitted to a straight line and the background above the edge was fitted with a cubic spline. The EXAFS function, χ, was obtained by subtracting the postedge background from the overall absorption and then normalized with respect to the edge jump step. The normalized $\chi(E)$ was transformed from energy space to k-space, where 'k' is the photoelectron wave vector. The $\chi(k)$ data were multiplied by k^2 to compensate the damping of EXAFS oscillations in the high k-region. Subsequently, k^2-weighted $\chi(k)$ data in the k-space ranging from 3.6 to 12.6 $Å^{-1}$ for the Pt L_{III}-edge, from 3.6 to 11.6 $Å^{-1}$ for the Ru K-edge were Fourier transformed (FT) to r-space to separate the EXAFS contributions from the different coordination shells. A nonlinear least-squares algorithm was applied to the curve fitting of an EXAFS in the r-space between 1.2 and 3.2 Å (without phase correction) for Pt, between 1.0 and 3.2 Å for Ru. The Pt-Ru reference file was determined by a theoretical calculation. All the computer programs were implemented in the UWXAFS 3.0 package [13] with the backscattering amplitude and the phase shift for the specific atom pairs being theoretically calculated by using FEFF7 code [14]. From these analyses, structural parameters like coordination numbers (N), bond distance (R), the Debye–Waller factor

($\Delta\sigma_j^2$), and inner potential shift (ΔE_0) have been calculated. The amplitude reduction factor, S_0^2, values for Pt and Ru were obtained by analyzing the Pt foil and Ru powder reference samples, respectively, and by fixing the coordination number in the FEFFIT input file. The S_0^2 values were found to be 0.905 and 0.880 for Pt and Ru, respectively.

2.5. Energy-dispersive X-ray spectroscopy (EDX) measurements

The EDX measurements were performed on the fresh and faded MEA with a JSM 6500 EDX analyzer to measure the composition changes before and after the DMFC operation.

2.6. Raman spectroscopy measurements

Raman spectra were recorded both on the fresh and faded MEA using a Renishaw inVia Raman spectrometer employing a diode laser of 10 mW radiating on the sample operating at 785 nm. A 50 × 0.75 NA Leica objective was used to focus the laser light on the samples. The laser spot size is ca. 1–2 μm. A thermoelectrically cooled charge-coupled device (CCD) with 1024 × 256 pixels operating at −60 °C was used as the detector with 1 cm^{-1} resolution and each scan takes 15 min.

3. Results and discussion

The polarization curves of a single cell DMFC measured before and after the 600 h lifetime testing are presented in Fig. 1. All fading studies were performed on the dried MEA after single cell DMFC operation for 600 h (hence in the preceding text after DMFC operation should be read as after operation of single cell DMFC for 600 h). As can be seen from Fig. 1, the open circuit voltage (OCV) was found to be approximately 0.53 V at the beginning of the cell operation. The OCV was found to be decreased to 0.50 V after the cell operation. The polarization curve after the cell operation showed a steeper fall in performance in the Ohmic polarization region compared to the curve of initial operation. In order to understand the fading factors of the MEA after DMFC operation, the components of the MEA including the anode layer, cathode layer, membrane, and gas diffusion layer analyzed by various techniques such as XRD, XAS, EDX, and Raman spectroscopy were presented as follows.

The high energy XRD measurements were conducted on the fresh and faded MEA at both the anode and cathode layers to identify the changes in the catalysts and were shown in the panel (a) and (b), respectively, of Fig. 2. The Pt characteristic peaks corresponding to Pt (1 1 1), Pt (2 0 0), and Pt (2 2 0) were observed in both the fresh and faded MEA at both the anode and cathode layers. The XRD pattern for the anode layer and the cathode layer of the faded MEA becomes broader and sharper, respectively, compared to its corresponding layer of the fresh MEA, implying that a decrease in the grain size of the anode catalyst but an increase in that of the cathode catalyst. The average grain size is calculated by a full-width at half-maxima

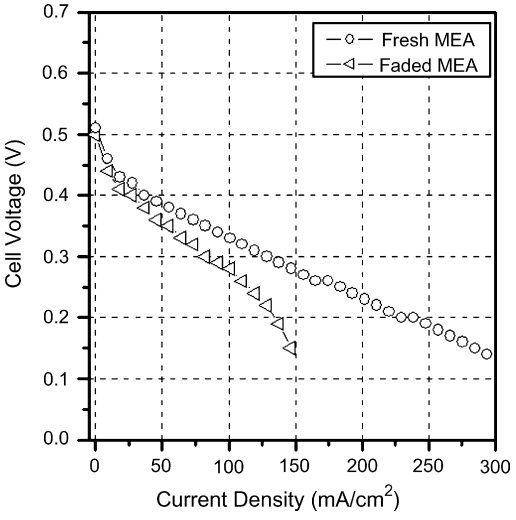

Fig. 1. Polarization curves of a DMFC single cell before and after 600 h of operation at 40 °C; CMeOH = 2.5 M, fMeOH = 0.366 cm^3 min^{-1}.

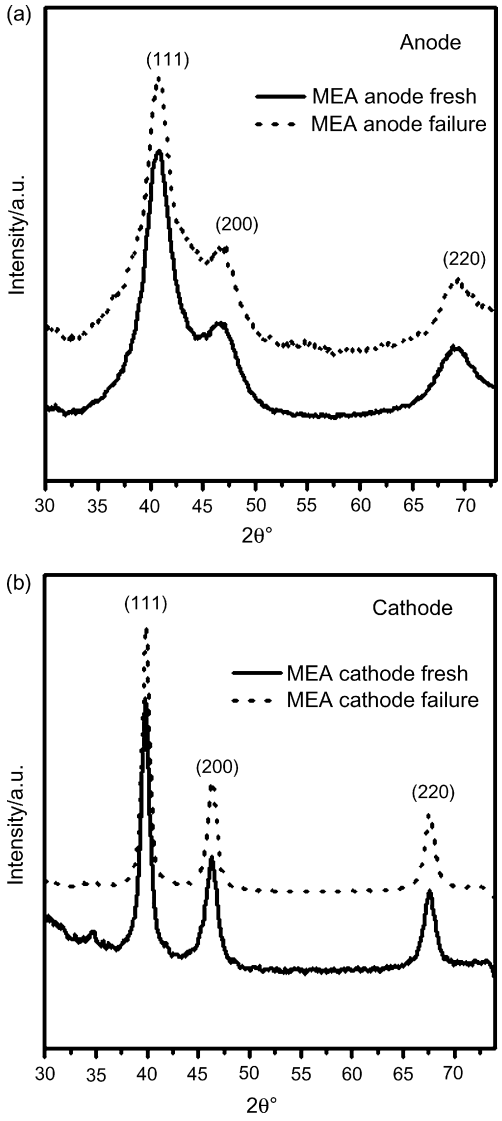

Fig. 2. High energy XRD spectra of fresh and faded MEA. (a) Anode side and (b) cathode side.

(fwhm) of the Pt (2 2 0) peak according to the Scherrer's equation in all the cases. In the case of anode catalyst of the fresh MEA the grain size of the catalyst was found to be 2.1 nm and it is decreased to 1.7 nm in the case of anode catalyst of the faded MEA. The particle size obtained from the averaged first shell coordination number from XAS results presented in the subsequent paragraphs is 2 nm for the anode catalyst of the fresh MEA is consistent with the XRD results. The decrease in grain size of the catalyst from fresh to the faded MEA may be attributed to the Ru loss from the catalyst during the DMFC operation. The observation of Ru loss from the Pt-Ru catalyst is evident from the XAS and EDX results which are provided in proceeding paragraphs. The grain size of the cathode catalyst in the fresh MEA is 6.5 nm and it is increased to 8.1 nm in the faded MEA. The increase in grain size results from the aggregation of the catalyst clusters or the deposition of Ru atoms on the clusters in the case of cathode layer of the faded MEA. The raise in grain sizes or the change in surface composition of the cathode catalysts of faded MEA may affect the reaction kinetics and ultimately degraded the cell performance. It is consistent with the previous lifetime testing results from a DMFC single cell [10].

To further analyze the structural changes in the electrocatalysts, XAS experiments were performed on the fresh and faded MEA at both anode and cathode layers. The Fourier transformed EXAFS spectra of anode layer of the fresh and faded MEA at Pt L_{III}-edge and at Ru K-edge were shown in the panel (a) and (b), respectively, of Fig. 3. As can be seen from Fig. 3(a), the spectra show splitting of a peak corresponding to the first coordination shell in the region 2–3 Å caused by the radiation backscattering from Pt and Ru neighbors. The EXAFS fitting parameters obtained for the fresh and faded MEA anode catalyst are shown in Table 1. For the fresh MEA anode the XAS results shows that the number of nearest neighbors around Pt and Ru are 9.3 and 5.9, respectively, giving an averaged first-shell coordination number of 7.6. This value corresponds to an average particle size of about 2 nm on the assumption of close packed structure. Both XRD and XAS results agreed well in estimating the particle size. The total coordination of Pt and Ru around Pt in the anode catalyst, i.e. $N_{Pt\text{-}Pt} + N_{Pt\text{-}Ru}$ decreases from 9.3 for the fresh MEA to 7.7 for the faded MEA in agreement with the decrease in the grain size of the anode in the faded MEA, as observed from the XRD. From Fig. 3(b) we can see that significant changes

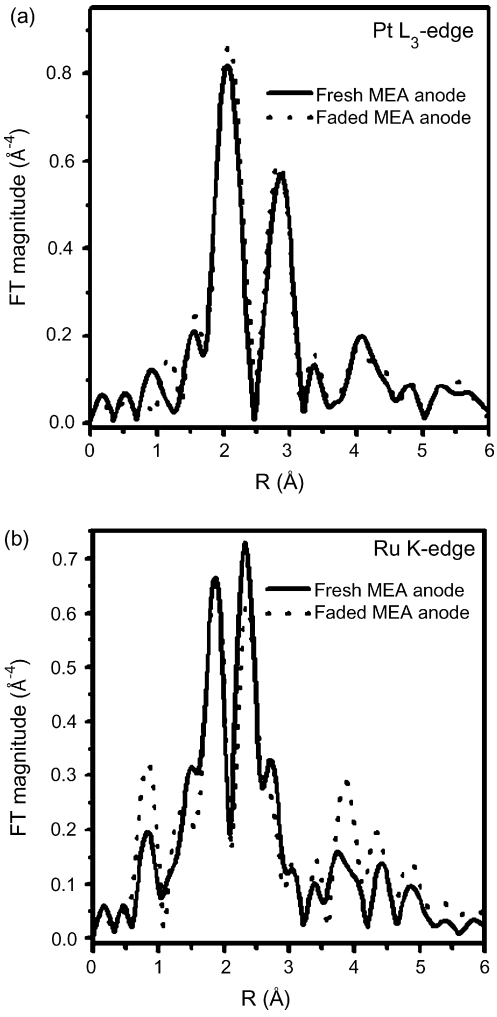

Fig. 3. Fourier transformed EXAFS spectra of anode side of fresh and faded MEA at: (a) Pt L_{III}-edge, and (b) Ru K-edge.

were occurred in the Ru K-edge FT EXAFS spectra of the faded MEA anode when compared to the fresh one. The Pt L_{III}-edge FT EXAFS spectra of the fresh MEA and faded MEA cathode are compared in Fig. 4. As can be seen from Fig. 4 the FT peak magnitude of the faded MEA cathode is higher than that of the fresh MEA cathode indicating the size or composition changes in the cathode catalyst of the faded MEA. These changes may

Table 1
EXAFS fit results for anode side of both fresh and faded MEA at both Pt L_{III} and Ru K-edges

Sample	Shell	N	R (Å)	σ_j^2(Å^2) × 10^{-3}	ΔE_0 (eV)	R-factor
Fresh MEA						
(Pt L_{III}-edge)	Pt-Ru	2.64 (±0.23)	2.69 (±0.008)	6.1 (±0.7)	2.24 (±0.14)	
	Pt-Pt	6.67 (±0.24)	2.74 (±0.007)	7.1 (±0.5)	5.86 (±0.21)	
(Ru K-edge)	Ru-Pt	2.64 (±0.23)	2.70 (±0.008)	4.7 (±0.6)	−10.32 (±0.064)	
	Ru-Ru	3.29 (±0.31)	2.66 (±0.005)	6.0 (±0.6)	−7.26 (±0.33)	0.0104
Faded MEA						
(Pt L_{III}-edge)	Pt-Ru	1.96 (±0.15)	2.69 (±0.007)	3.6 (±0.7)	2.76 (±0.22)	
	Pt-Pt	5.70 (±0.21)	2.72 (±0.006)	5.7 (±0.6)	4.20 (±0.20)	
(Ru K-edge)	Ru-Pt	2.45 (±0.21)	2.69 (±0.005)	4.1 (±0.4)	−11.32 (±0.71)	
	Ru-Ru	2.81 (±0.23)	2.68 (±0.004)	5.3 (±0.6)	−5.92 (±0.42)	0.0257

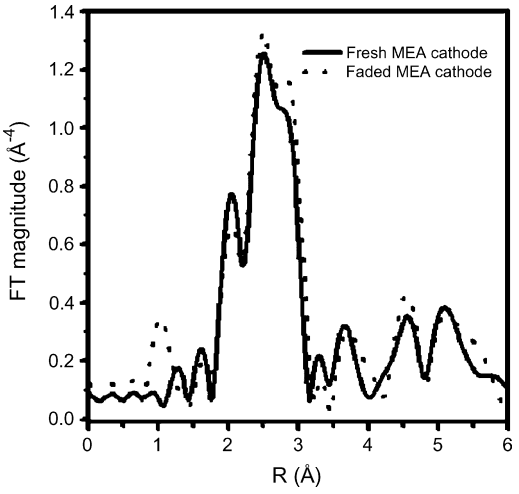

Fig. 4. Pt L_{III}-edge FT-EXAFS spectra of cathode side of fresh and faded MEA.

result from the Ru crossover and its re-deposition/or accumulation on the surface of Pt clusters or the aggregation of Pt clusters. From the XAS fitting results it is observed that the Ru coordination around Pt ($N_{Pt\text{-}Ru}$) and around Ru ($N_{Ru\text{-}Ru}$) as 2.64 and 3.29, respectively, for the fresh MEA anode is decreased to 1.96 and 2.81, respectively, in the faded MEA anode. The decrease in Ru the coordination around both Pt and Ru can be attributed to the Ru dissolution from the catalyst. Previous researchers have provided evidence for the Ru dissolution from the Pt-Ru catalyst during DMFC operation based on X-ray fluorescence analysis and attributed the Ru dissolution from the Pt-Ru catalyst to the thermodynamic instability of elemental Ru under DMFC operation conditions [15]. Smotkin and co-workers have reported the substantial loss of Ru from Johnson Matthey Pt-Ru catalyst and Reetz Pt-Ru catalyst containing MEA surfaces during DMFC operation based on X-ray photoelectron spectroscopy [16]. However, to the best of our knowledge the XAS evidence of ruthenium dissolution from Pt-Ru catalyst is not reported so far.

The alloying extent of Pt (J_{Pt}) and Ru (J_{Ru}) in the Pt-Ru catalyst NPs of both the fresh and the faded MEA anode is calculated by our developed XAS methodology [17] and the structural parameters needed to calculate J_{Pt} and J_{Ru} are derived by utilizing the coordination numbers of Pt and Ru of Table 1 and listed in Table 2. The total coordination number of Pt and Ru around Pt ($\Sigma N_{Pt\text{-}i} = N_{Pt\text{-}Pt} + N_{Pt\text{-}Ru}$) is found to be 9.31 and 7.66 for the fresh and the faded MEA anode, respectively. Similarly, the total coordination number of Ru and Pt atoms around the Ru ($\Sigma N_{Ru\text{-}i} = N_{Ru\text{-}Ru} + N_{Ru\text{-}Pt}$) is determined as 5.93 and 5.26, respectively, for the fresh and the faded MEA anode. From these values the structural parameter $P_{observed}$ ($N_{Pt\text{-}Ru}/\Sigma N_{Pt\text{-}i}$) and $R_{observed}$ ($N_{Ru\text{-}Pt}/\Sigma N_{Ru\text{-}i}$) was calculated as 0.284 and 0.445, respectively, for the fresh MEA anode and 0.256 and 0.466, respectively, for the faded MEA anode. Then the alloying extent of Pt (J_{Pt}) and Ru (J_{Ru}) values are calculated by using the Eqs. (1) and (2), respectively.

Table 2
XAS structural parameters and alloying extent of Pt (J_{Pt}) and Ru (J_{Ru}) of fresh and faded MEA anode

Sample	$\Sigma_{Pt\text{-}i}$	$\Sigma_{Ru\text{-}i}$	$P_{observed}$	$R_{observed}$	J_{Pt} (%)	J_{Ru} (%)
Fresh MEA	9.31	5.93	0.284	0.445	49.6	89.0
Faded MEA	7.66	5.26	0.256	0.466	58.2	83.2

$$J_{Pt} = \frac{P_{observed}}{P_{random}} \times 100 \quad (1)$$

$$J_{Ru} = \frac{R_{observed}}{R_{rsandom}} \times 100 \quad (2)$$

where P_{random} and R_{random} can be taken as 0.5 for perfect alloyed bimetallic NPs if the atomic ratio of 'Pt' and 'Ru' is 1:1. This value can be achieved by assuming $N_{Pt\text{-}Pt} = N_{Pt\text{-}Ru}$ and $N_{Ru\text{-}Ru} = N_{Ru\text{-}Pt}$ which is generally true for the perfect alloyed bimetallic NPs. However in the present investigation the P_{random} and R_{random} values used for the fresh MEA anode are 0.572 and 0.500, respectively, and for the faded MEA anode are 0.440 and 0.560, respectively, and were calculated based on the Pt and Ru edge jump measurements. By using the Eqs. (1) and (2) the alloying extent of Pt (J_{Pt}) and Ru (J_{Ru}) values are calculated as 49.6 and 89.0%, respectively, for the fresh MEA anode and 58.2 and 83.2% for the faded MEA anode. The observed parameters showing $\Sigma N_{Pt\text{-}i} > \Sigma N_{Ru\text{-}i}$ and $J_{Ru} > J_{Pt}$ indicates that the Pt-Ru/C NPs adopt a Pt rich in core and Ru rich in shell structure for the Pt-Ru NPs of both the fresh and the faded MEA anode. The observed parameter relationship, i.e. $\Sigma N_{Pt\text{-}i} > \Sigma N_{Ru\text{-}i}$ for the Pt-Ru/C nanoparticles investigated here is consistent with the relationship $N_{AA} + N_{AB} > N_{BA} + N_{BB}$ for a homogeneous system of A–B bimetallic NPs for which the core of the cluster is composed of N atoms of A (N_A) and the surface is made of N atoms of B (N_B), the total coordination number ($N_{AA} + N_{AB}$) for the 'A' atom and greater than the total coordination for the 'B' atoms ($N_{BA} + N_{BB}$) [18–20]. The decrease in alloying extent of Ru (J_{Ru}) from the fresh to the faded MEA suggests that during prolonged hours of operation Ru is dissolved from the Pt-Ru catalyst. The observed decrease in (J_{Ru}) may suggest that the Ru dissolution takes place from the one which is preferentially heterometallic bonding with Pt atoms. It suggests that the fading of the Pt-Ru electrocatalysts can be inhibited by stabilizing the Ru in the catalyst. We speculate that the dissolution of Ru under fuel cell operation conditions may enhance the mobility of Pt in the Pt-Ru matrix and hence an alteration of Pt distribution can be expected. The observed increase in alloying extent of Pt (J_{Pt}) from the fresh to the faded MEA anode supports this speculation. Previous studies of fuel cell electrodes with carbon supported platinum catalysts showed the platinum mobility under fuel cell conditions [21,22]. Hence, we believe that in the Pt-Ru catalyst of the faded MEA anode, Ru is dissolved from the Pt-Ru clusters and Pt is moved to the shell region and the resulting structure of the fresh and the faded MEA anode Pt-Ru catalyst is shown in Fig. 5.

Further evidence for this observation can also be obtained from the compositional changes in the Pt-Ru black catalyst of the fresh and faded MEA anode calculated from XAS by measuring the edge jump ($\Delta\mu x$) at the Pt L_{III}-edge and the Ru K-edge. It is found that the Pt:Ru atomic ratio is 1:1 and 1:0.8 for the fresh and

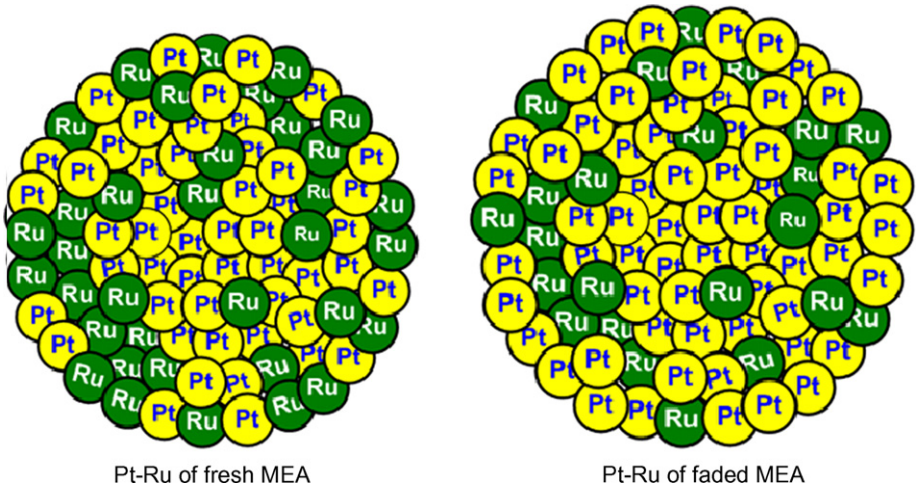

Fig. 5. Schematic representation of Pt-Ru catalyst NPs of fresh and faded MEA anode.

faded MEA anode, respectively indicating that Ru is dissolved from the Pt-Ru catalyst during fuel cell operation. In case of the MEA cathode, the edge jump results show Pt:Ru atomic ratio as 1:0 and 1:0.04 for the fresh and faded MEA, respectively. This result suggests the presence of Ru at the cathode of the faded MEA. The EDX analyses were also performed on the anode catalyst layers of the fresh and the faded MEA. The atomic ratio of Pt:Ru obtained from EDX analysis is 1:1 and 1:0.7 for the fresh and faded MEA anode, respectively, which is in good agreement with the XAS results.

The *F*/*C* atomic ratio is the key factor for obtaining the hydrophobic nature of the gas-diffusion layers (GDL). The energy-dispersive X-ray analysis was suitable to determine the atomic ratio and chemical environment of the GDLs. Here, EDX measurements were performed on the GDL of the fresh and the faded MEA. The measured data are shown in Table 3. As shown in this table, the *F*/*C* atomic ratio of GDL of the faded MEA in the anode side increases when compared to the GDL of the fresh MEA. The increased *F*/*C* atomic ratio of the GDL for the faded MEA can be taken as an indication to its increased hydrophobicity. In the case of the GDL of the faded MEA in the cathode side the *F*/*C* atomic ratio is decreased. As the cathode GDL is used the PTFE coating it may be degraded via radical attack under electrochemical conditions. During the decomposition of

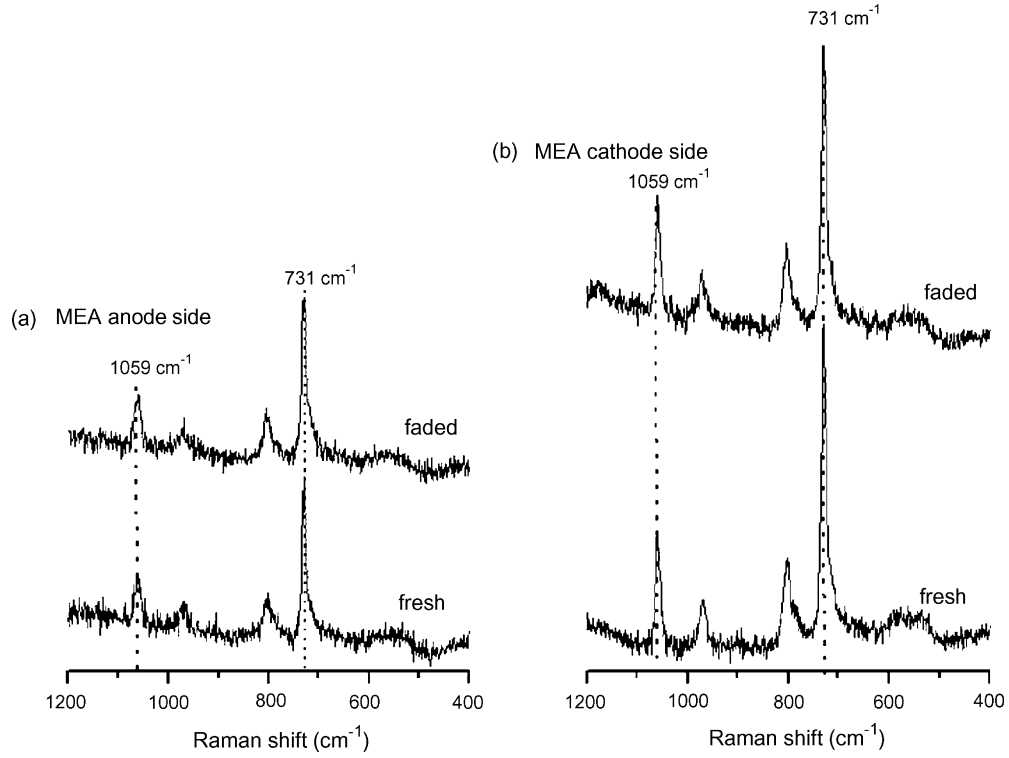

Fig. 6. Raman spectral features measured for the membrane of fresh and faded MEAs exposed to (a) anode and (b) cathode sides.

Table 3
EDX analysis of both anode and cathode side gas-diffusion layer (GDL) of fresh and faded MEA

Sample	Atomic ratio of *F*/*C*
GDL of fresh MEA	0.43
Anode GDL of faded MEA	1.25
Cathode GDL of faded MEA	0.25

PTFE the ratio between fluorine and carbon decreases and it can be typically related to a loss of the hydrophobic nature of the cathode GDL. The increase in the *F*/*C* ratio in the anode GDL may result from the migration of the binder of Nafion ionomer from the anode layer to the GDL. Both changes contribute to the performance degradation of the fuel cell.

Raman spectroscopy provides valuable information on structural changes in proton exchange membranes and several issues such as, membrane composition, molecular coordination, and polymer conformation can be studied. An added strength of Raman spectroscopy is that under optimized conditions the spatial resolution obtained is on the level of micrometers both in horizontal and depth directions. The spatial resolution has for instance been exploited to map the distribution of functional molecular groups in a membrane [23] or to follow the extent of degradation of fuel cell tested membranes ex situ [24–26]. We recorded Raman spectra of both the fresh and the faded MEA membrane exposed to the anode layer as well to the cathode one and were shown in Fig. 6. The intensity of the Nafion vibrations at 802 and 969 cm^{-1} is assigned to the symmetric stretch of ν(C–S) and ν_s(C–O–C) bands, respectively. Similarly the intensity of the Nafion vibrations at 731 and 1059 cm^{-1} is assigned to the symmetric stretch of CF_2 and $SO_3{}^-$, respectively [27,28]. Therefore, the change in the ratio of band intensities for 1059 cm^{-1} ($SO_3{}^-$) and 731 (CF_2), I_{1059}/I_{731}, indicates the extent of chemical degradation of Nafion membranes. The value of I_{1059}/I_{731} was calculated to be 0.35 for the fresh MEA membrane exposed to the anode layer and the value is not changed even after 600 h of fuel cell operation. However the value of I_{1059}/I_{731} is of about 0.30 for fresh MEA membrane exposed to the cathode layer and it is increased to 0.36 after fuel cell operation. This result indicates that the degradation of membrane exposed to the cathode layer is more serious than the membrane exposed to the anode one. These changes are significant to realize the membrane degradation.

4. Conclusions

Preliminary DMFC life time tests were carried out and the electrocatalyst layers, gas-diffusion layers and membrane from fresh and faded MEAs were characterized by high energy XRD, XAS, EDX and Raman spectroscopic techniques. The XRD analysis showed that the mean particle size of cathode catalysts became larger when compared to the anode after prolonged fuel cell operation. The XAS results reveal that Ru is dissolved from the Pt-Ru catalyst during life time tests. The XAS edge jump measurements confirm the presence of Ru in cathode side of faded MEA. It appears that once Ru is deposited at the cathode, ruthenium inhibits oxygen reduction kinetics and the catalyst ability to handle methanol crossover. The *F*/*C* atomic ratio obtained from EDX analysis of fresh and faded MEA reveals that the hydrophobic nature of cathode is decreased in faded MEA and hydrophobicity of anode is increased after fuel cell operation. We found that the membrane degradation under fuel cell conditions is accelerated at the cathode side. However membrane failure is caused by a great number of interacting factors of both chemical and physical origin and studies to clarify the degradation mechanisms are the scope of our future works.

Acknowledgements

The authors gratefully acknowledge the financial support of Industrial Technological Research Institute (ITRI), National Science Council, facilities from the National Synchrotron Radiation Research Center (NSRRC), and the National Taiwan University of Science and Technology, Taiwan, ROC.

References

[1] S. Wasmus, W. Vielstich, J. Appl. Electrochem. 23 (1993) 120.
[2] X. Ren, M.S. Wilson, S. Gottesfeld, J. Electrochem. Soc. 143 (1996) L12.
[3] L. Carrette, K.A. Friedrich, U. Stimming, Fuel Cells 1 (2001) 5.
[4] A.S. Arićo, S. Srinivasan, V. Antonucci, Fuel Cells 1 (2001) 133.
[5] S. Wasmus, A. Küver, J. Electroanal. Chem. 14 (1999) 461.
[6] X.M. Ren, P. Zelenay, J. Davey, S. Gottesfeld, J. Power Sources 86 (2000) 111.
[7] M. Baldauf, W. Preidel, J. Appl. Electrochem. 31 (2001) 781.
[8] S.C. Thomas, X. Ren, S. Gottesfeld, P. Zelenay, Electrochim. Acta 47 (2002) 3741.
[9] A.K. Shukla, C.L. Jackson, K. Scott, R.K. Raman, Electrochim. Acta 47 (2002) 3401.
[10] J. Liu, Z. Zhou, X. Zhao, Q. Xin, G. Sun, B. Yi, Phys. Chem. Chem. Phys. 6 (2004) 134.
[11] See for example the guidelines for data collection modes for EXAFS measurements and user-controlled parameters at http://ixs.iit.edu/subcommittee_reports/sc/sc00report.pdf.
[12] Guidelines for errors reporting can be found at http://ixs.iit.edu/subcommittee_reports/sc/err-rep.pdf.
[13] F.A. Stern, M. Newville, B. Ravel, Y. Yacoby, D. Haskel, Physica B 208–209 (1995) 117.
[14] S. Zabinsky, J.J. Rehr, A.L. Ankudinov, R.C. Albers, M. Eller, J. Phys. Rev. B 52 (1995) 2995.
[15] P. Piela, C. Eickes, E. Brosha, F. Garzon, P. Zelenay, J. Electrochem. Soc. 151 (2004) A2053.
[16] R.R. Díaz-Morales, R. Liu, E. Fachini, G. Chen, C.U. Segre, A. Martínez, C. Cabrera, E.S. Smotkin, J. Electrochem. Soc. 151 (2004) A1314.
[17] B.J. Hwang, L.S. Sarma, J.M. Chen, C.H. Chen, S.C. Shih, G.R. Wang, D.G. Liu, J.F. Lee, M.T. Tang, J. Am. Chem. Soc. 127 (2005) 11140.
[18] D. Bazin, D. Sayers, J.J. Rehr, J. Phys. Chem. B 101 (1997) 11040.
[19] G.H. Via, J.H. Sinfelt, in: Y. Iwasawa (Ed.), X-ray Absorption Fine Structure for Catalysts and Surfaces, World Scientific, London, 1996.
[20] J. Moonen, J. Slot, L. Lefferts, D. Bazin, H. Dexpert, Physica B 208–209 (1995) 689.
[21] P. Staiti, A.S. Aricó, V. Antonucci, S. Hocevar, J. Power Sources 70 (1998) 91.
[22] K.F. Blurton, H.R. Kunz, D.R. Rutt, Electrochim. Acta 23 (1978) 183.
[23] B. Mattson, H. Ericson, L.M. Torell, F. Sundholm, J. Polym. Sci. Part A: Polym. Chem. 37 (1999) 3317.
[24] B. Mattson, H. Ericson, L.M. Torell, F. Sundholm, Electrochim. Acta 45 (2000) 1405.

[25] H. Ericson, T. Kallio, T. Lehtinen, B. Mattson, G. Sundholm, F. Sundholm, P. Jacobson, J. Electrochem. Soc. 149 (2002) A206.
[26] T. Kallio, K. Jokela, H. Ericson, R. Serimaa, G. Sundholm, P. Jacobson, J. Appl. Electrochem. 33 (2003) 505.
[27] A. Gruger, A. Regis, T. Schmatko, P. Colomban, Vibr. Spectrosc. 26 (2001) 215.
[28] H. Matic, A. Lundblad, G. Lindbergh, P. Jacobsson, Electrochem, Solid State Lett. 8 (2005) A5.